System components for laser free confocal Microscopy

T. Wilson*[a], G. Holst[b], K. Aswami[c]

[a]Aurox Ltd, Culham Campus, Abingdon, OX14 3DB, UK; [b]Excelitas PCO GmbH, Donaupark 11, 93309 Kelheim, Germany; [c]Excelitas 2260 Argentia Road, Mississauga L5N6H7, Canada

ABSTRACT

Confocal microscopy enables high resolution, high contrast, optical sectioned imaging of thick specimens by rejecting out-of-focus light. While the confocal optical architecture provides the necessary confocal sectioning it is necessary both to use a bright light source such as a laser and to introduce scanning to image an extended region of the specimen. Fortunately, technical advances in areas such as high-quality sCMOS cameras, non-laser (LED) light sources and inexpensive optical image processing has permitted alternative, 21st century, approaches to obtain optical sectioning to be developed. We will describe the factors influencing the choice of light source and camera in one such implementation which uses a combination of structured illumination and structured detection to produce the optical sectioning.

Keywords: Confocal microscopy, scientific cameras, sCMOS camera, laser-free confocal, microscope light sources

1. INTRODUCTION

The most important property of the confocal microscope is probably its ability to record high resolution, high contrast, in-focus images of thin slices from within a thick specimen. In many cases, the increase in contrast in these image slices is the important point. In other cases, taking a through-focus series of such optical sections allows computer rendering of the specimen in three dimensions. The original designs of such instruments used the point source – point detector optical system proposed by Marvin Minsky in the 1950s. This optical architecture provides the necessary optical sectioning but, in order to form an image, it is necessary both to introduce scanning and, because of the need to use point illumination, a bright light source such as a laser must also be used. This was the only practical approach when confocal microscopy first came to prominence in the 1970s. The early systems, and many commercial implementations, were (and still are) built around conventional microscopes. However, since these early days technological advances in areas such as high-quality CCD cameras, non-laser light sources and inexpensive optical image processing has permitted alternative, 21st century, approaches to obtain optical sectioning to be developed. We will describe one such approach which uses a combination of structured illumination and structured detection to allow optical sectioning to be achieved at high speed without the need for laser illumination. The approach can either be combined with a conventional optical microscope or built as a stand-alone system.

*tony.wilson@aurox.co.uk; phone +44 07712044986; www.aurox.co.uk

Three-Dimensional and Multidimensional Microscopy: Image Acquisition and Processing XXXIII, edited by Thomas G. Brown, Tony Wilson, Laura Waller, Proc. of SPIE Vol. 13857, 138570A
2026 Published by SPIE · 1605-7422 · doi: 10.1117/12.3079981

2. OPTICAL SECTIONING

Optical sectioning, as we have said, has traditionally been achieved by using the confocal point source – point detector optical architecture. In this optical system light from a point source of light is focused to a diffraction limited spot in a specimen. The reflected (or fluorescent) light from this object point is then measured by a photo detector placed behind an on-axis detector pinhole positioned in a plane conjugate to that of the source. The system achieves optical sectioning since the detector pinhole prevents -- physically blocks -- light originating from out of focus planes from reaching the photo detector and hence contributing to the detected signal, Figure 1 (a).

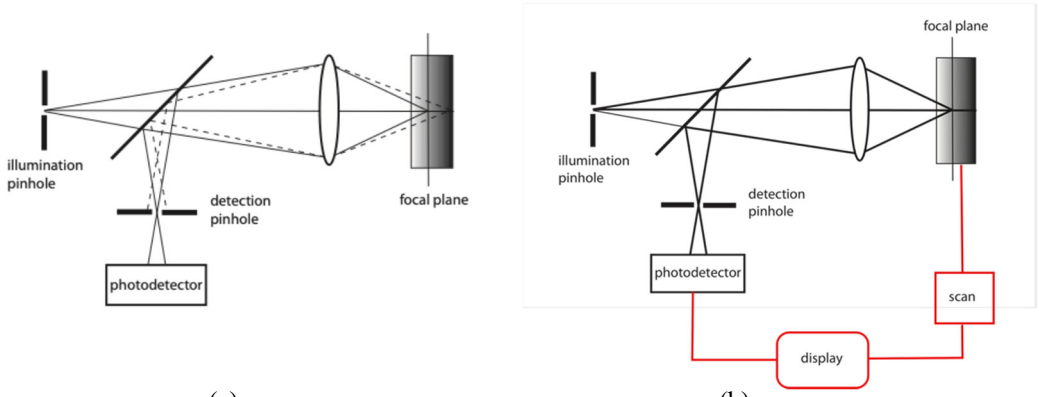

Figure 1. Figure 1 (a) shows the origin of optical sectioning in the point source -- point detector confocal geometry whereas Figure 1(b) emphasizes the need to introduce scanning in order to image an extended region of a specimen.

Although this system provides optical sectioning by preferentially detecting signal from the focal region it suffers from two problems when applied to microscopy. First of all, and perhaps most importantly, the system just described does not form an image since it probes only one point. In order to form an image of an extended region of the specimen, some form of scanning must be introduced, Figure 1(b). Additionally, since point source illumination is required, it is not possible to use a standard microscope illuminator and one must resort to using brighter light sources. Typically laser illumination is employed although no other properties of the laser are usually taken advantage of.

There are two approaches to implementing the scanning. The first uses a single confocal system together with laser illumination and a mechanism to scan the focused spot with respect the specimen. The second approach, which also requires laser illumination, uses multiple confocal systems in parallel in a reciprocal geometry. The advantage of this arrangement, where the same pinhole is used as both source and detector, is that it allows the simultaneous imaging of neighbouring points in the specimen. However, since the role of the detector pinhole is to physically block light from out of focus regions, it is necessary that the individual confocal systems in this parallel implementation are spaced sufficiently far apart that the out of focus light from one confocal system is not detected by its neighbour. This requirement leads to a dramatic reduction in the light efficiency, hence the need for bright laser illumination. Further, the need that the neighbouring confocal systems be widely separated leads to the additional drawback that the specimen sparsely probed. In order to overcome these problems, the pin holes are typically arranged in interweaving Archimedian spirals and impressed on a disk which then needs to be spun in order to 'fill in the gaps' and image the whole specimen.

As we have seen when the confocal microscope came to prominence in the 1970s, these were the only practical approaches. We now show how the considerable technological advances in the development of sensitive scientific cameras and enhanced LED based illumination sources have allowed alternative, more light efficient, approaches to obtaining optical sectioning to be adopted.

3. ALTERNATIVE APPROACHES

We begin with a clean sheet of paper and suppose that we can label a thin section – an optical section -- within the volume of a specimen. The image which a camera would record in a conventional microscope would consist of the labelled optical section – the labelled confocal image -- together with a background image. We could write this as

$$I = I_{\text{background}} \; + \; [I_{\text{section}}]_{\text{labelled}} \tag{1}$$

In order to adopt this approach, it is necessary to devise a method to label the optical section as well as to decide how to extract the desired optical section (confocal image) from within the recorded composite image. Conceptually, the demodulation of the recorded composite image might begin by removing the background image so as to leave the labelled optical section. The final step in the process would be to find a way to remove the label and hence reveal the optical section.

We will now describe two implementations of this idea[1] which, as we will see, is sufficiently light efficient that we do not need to resort to laser illumination; LED microscope illuminators are perfectly adequate.

Labelling via structured illumination

Since it is necessary that the labelling process be non invasive we elect to label the specimen with the image of a sinusoidal grid pattern. We choose this pattern since, as will be shown, via appropriate choice of the spatial frequency of the sinusoid, the imaged 'line pattern' (the label) only has high contrast in regions close to the focal plane. In order to illustrate this, we consider the incoherent image of a mask of the form

$$I(x_0) = 1 + m\cos(2\pi f x_0) \tag{2}$$

This mask, defined by its modulation depth, m, spatial frequency, f, which is related to its pitch, Λ, by $f = \frac{1}{\Lambda}$, is imaged incoherently to the specimen plane where it excites fluorescence in the specimen according to

$$I(x_1) = 1 + m\, C(u, f)\cos(2\pi f x_1) \tag{3}$$

where $C(u, f)$ is the incoherent transfer function. Figure 2 (a) shows this function in terms of a normalised special frequency, $v = f\,\frac{\lambda}{n\sin\alpha} = f\,\frac{\lambda}{\text{NA}}$ where $n\sin\alpha$ denotes the numerical aperture, NA. The various curves are drawn for increasing amounts of defocus, z, characterised by the dimensionless unit $u = 4\,kn\,z\,\sin^2(\alpha/2)$. We see that by choosing an appropriate spatial frequency of the illumination grid, f, we can ensure that the modulation decreases with increasing defocus. This point is further emphasised in Figure 2 (b) where the same information is presented as a function of defocus for a few chosen normalised source spatial frequencies.

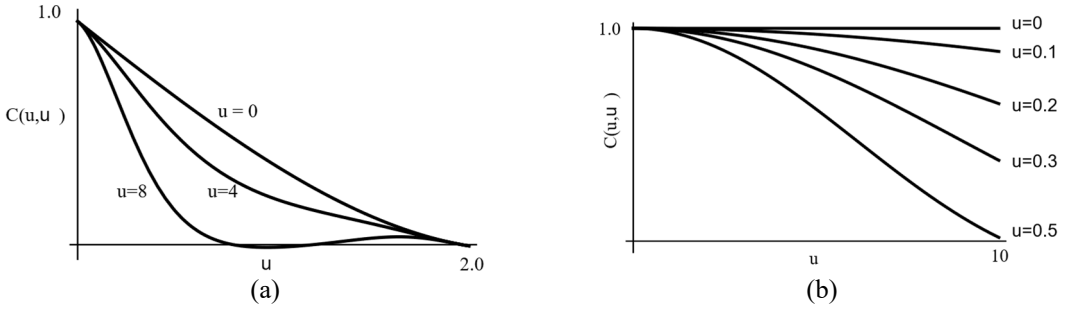

Figure 2. Figure2 (a) shows incoherent transfer function as a function of spatial frequency for specific values of the focus whereas Figure 2(b) shows the same information but as a function of defocus for specific values of special frequency

In order to further emphasizes the point we show, Figure 3, the image of the sinusoidal mask for varying degrees of defocus. This is the pattern which is superimposed the specimen to act as a label for the optical section. As can be seen the label is visible with high contrast only in planes close to focus and hence only the regions of the volume specimen close to the plane of focus of this mask will be labelled.

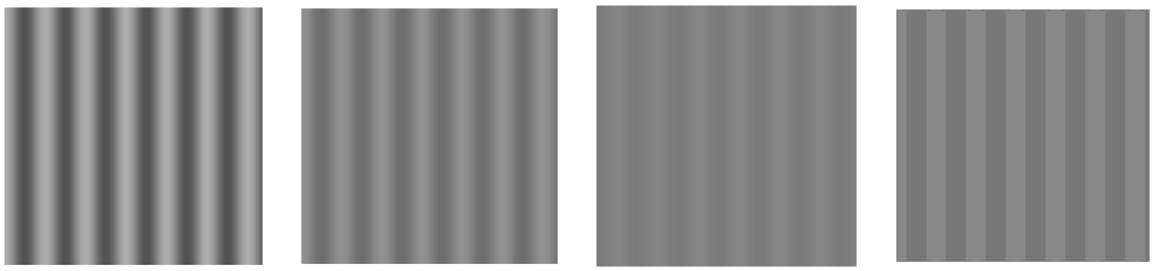

Figure 3. The left figure shows the in-focus image of the sinusoidal mask. The other images correspond to normalized defocus settings of $u = 5,10,15$.

The composite image

The specimen, labeled with the line pattern derived from the image of a sinusoidal grid, is now imaged in a conventional microscope imaging system to form a composite image consisting of a background image together with the desired, labeled, optical section. We will not present a full theory of the image formation here, but rather specialize to the case where the specimen consists of a thin fluorescent sheet. We choose this specimens since the imaging of such specimens is fundamental to understanding and characterizing the strength of optical sectioning. In the conventional microscope the image of such a planar specimen does not change with defocus, $C(0,u) = 1, \forall\, u$. There is no optical sectioning. In the confocal microscope, on the other hand, the intensity in the image of such a specimen decreases with defocus. The rate at which the intensity falls with defocus, depends on the size of the pinhole employed. It is greatest with the smallest possible pinhole, and the rate of decrease in intensity falls away as the pinhole becomes larger and, of course, the effect disappears altogether as the pinhole becomes infinitely large, and the imaging becomes identical to that of a conventional microscope. This 'axial response' has become an accepted method of both illustrating and characterizing the optical sectioning effect (as well as highlighting aberrations in objective lenses). However, as useful as this measurement is, care must be exercised in extrapolating measurements from such a (zero spatial frequency) specimen to a real specimen consisting of a wide range of spatial frequencies. That said, since it is the specimen of choice for a discussion of optical sectioning, we will limit our analysis in this paper to such specimen.

If we use the image of a mask with sinusoidal transmission then fluorescent in the specimen is excited by an intensity

$$I(x_1) = 1 + m\, C_1(u,f) \cos(2\pi f(x_1 + \phi)) \tag{4}$$

This is equivalent to equation (2) but with a phase shift ϕ to describe the spatial position of the mask with respect of the specimen. $C_1(f,u)$ denotes the transfer function evaluated at the excitation wavelength λ_1. If we restrict ourselves to a specimen, consisting of a thin fluorescent sheet then the intensity in the image plane is given by

$$I(x_2) = 1 + m\, C_1(u,f) C_2(u,f) \cos(2\pi f(x_2 + \phi)) \tag{5}$$

where $C_2(f,u)$ denotes the transfer function evaluated at the emission wavelength λ_2.

4. DEMODULATION

We may recognize the constant in Equation (5) as equivalent to the background, the factor $C_1(f,u)C_2(f,u)$ whose value decreases with (increasing) defocus, as the desired optical section and the cosine function represents the label. We must now decide how to remove the background and the label from this composite raw image. We will describe two approaches.

Computation

Since the phase, ϕ, essentially describes the lateral position of the mask with respect to the optical system it is straightforward to take a number of images at different positions (values of ϕ) and hence extract both the background and optically sectioned images. As an example if three images, I_1, I_2, I_3, are recorded at mask positions corresponding to $\phi = 0,\ {}^{\pi}/_{3}\ ,{}^{2\pi}/_{3}$, then the sectioned image may be extracted according to

$$I_{\text{section}} = \sqrt{(I_1 - I_2)^2 + (I_1 - I_3)^2 + (I_3 - I_2)^2} \tag{6}$$

and the background (conventional) image is revealed as

$$I_{\text{background}} = I_1 + I_2 + I_3 \tag{7}$$

This approach is very attractive since it simply requires a paddle containing the mask to be inserted in the illumination arm of a standard microscope, Figure 4 and, although this system can work well, there are drawbacks. The most obvious, perhaps, being that in order to appropriately excite fluorescence the condenser lens is required to image the mask onto the specimen. Unfortunately condenser lenses are not designed to act as imaging elements. Further, in order for the algorithms such as the one given above, or indeed any equivalent expressions, it is necessary to know precisely the relative values of ϕ. Any inaccuracies in these values will lead to failure, to some degree, of the reconstruction. Similarly, specimen movement between the recording of the images will lead to motion artifacts being visible in the reconstruction. Further objections might take the form of the non-linearity of the processing and the one dimensionality of the illumination leading to non-isotropic imaging. These problems may be addressed in the following implementation.

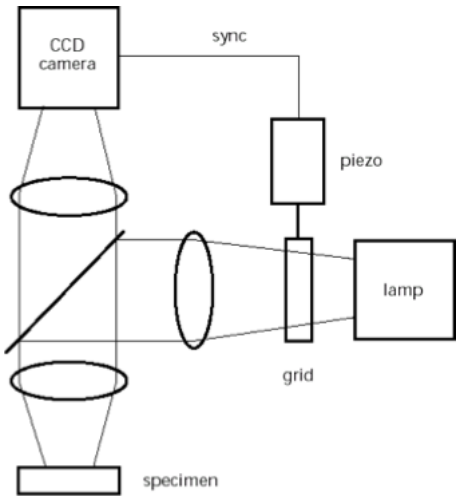

Figure 4. Schematic indicating positioning of a paddle containing the sinusoidal mask.

Structured illumination combined with structured detection

A better solution, which does not rely on the accurate knowledge of specific values of ϕ and processes the images in a linear fashion is to allow the image to pass back through a mask similar to the one used to create the structure of the sinusoidal illumination pattern. This leads to an image which may be written as.

$$I_{\text{T}}(x_2) = I(x_2)[1 + m\cos(2\pi f(x_1 + \phi))] \tag{8}$$

If we now move the mask in such a way that we essentially average over all values of ϕ then the image detected by the camera may be written

$$< I_{\mathrm{T}} >= 1 + m^2\, C_1(u,f)C_2(u,f) \tag{9}$$

We may also take advantage of the light reflected from the disk, which may be written as

$$I_{\mathrm{R}}(x_2) = \; I(x_2)[1 - m\cos(2\pi f(x_1 + \phi))] \tag{10}$$

and, hence

$$< I_{\mathrm{R}} >= 1 - m^2\, C_1(u,f)C_2(u,f) \tag{11}$$

It is then a simple matter to add these two images to obtain the background image and to reveal, by subtraction, the optically section image. In the case of our planar specimen, the optical sectioning is characterized by the behaviour of this image with defocus.

$$I_{\mathrm{section}}(u) \; = C_1(u,f)C_2(u,f) \tag{12}$$

In order to more easily interpret this result we introduce the normalized spatial frequency of the sinusoidal illumination pattern, $\bar{f}$, which, taking into account the magnification of the lens, M, is given by, $\bar{f} = f\,\frac{\lambda}{M\,\mathrm{NA}}$. We do this so that we may take advantage of an approximation to the transfer function $C(u,v)$ given by

$$C(u,v) \; = f(v)\left\{2\frac{J_1\left[uv(1 - {}^{v}/_{2}\right]}{\left[uv(1 - {}^{v}/_{2}\right]}\right\} \tag{13}$$

where

$$f(v) = 1 - 0.69v + 0.0076v^2 + 0.043v^3 \tag{14}$$

This allows us to write the optical sectioning strength, for the case of equal excitation and emission wavelengths, as

$$I(u) = C^2\left(u,\bar{\bar{f}}\right) \sim \left\{2\frac{J_1\left[u\bar{f}(1 - {}^{\bar{f}}/_{2}\right]}{\left[u\bar{f}(1 - {}^{\bar{f}}/_{2}\right]}\right\}^2 \tag{15}$$

If we take the full width at half maximum (FWHM) of this curve as an indication of the optical sectioning strength we can write, in optical coordinates, noting that $\left\{2\frac{J_1(x)}{x}\right\}^2 = 0.5$ when $x = 1.616$

$$u_{1/2} \; = \frac{3.232}{\bar{f}(1 - \bar{f}/2)} \tag{16}$$

which has a maximum value of 3.23 optical units maximum at $\bar{f} = 1$. We know that the corresponding half width for a point source-point detector confocal with infinitely small pin holes is 4.4 optical units and 6.0 optical units for an infinitely narrow slit detector. Figure 5 shows the behaviour. We also note that at large arguments $I(u) \sim {}^{1}/_{u^3}$ since the envelope of $J_1(x)$ at large argument varies as $\sqrt{\frac{2}{\pi x}}$

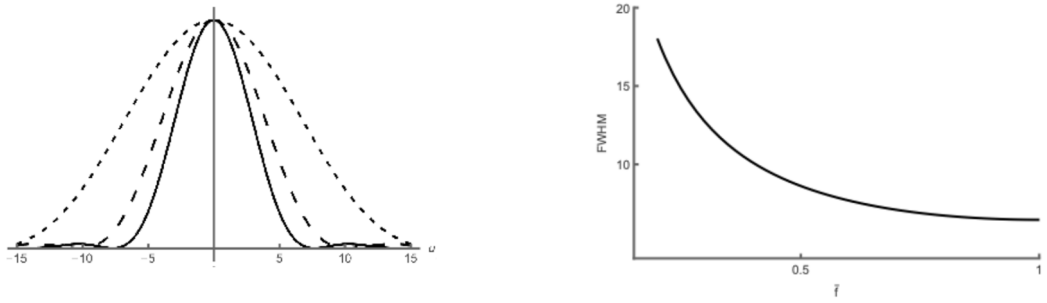

(a) (b)

Figure 5. The axial responses are shown for grid spacing corresponding to $\bar{f} = 1$ (full line), $\bar{f} = 0.5$ (long dashes), and $\bar{f} = 0.25$ (short dashes line) are shown in Figure 5(a). The FWHM of these curves as a function of normalized spatial frequency $\bar{f}$ are shown in Figure 5(b).

5. SYSTEM COMPONENTS

There are many ways in which the structured illumination/ structured detection method of obtaining optical sectioning can be implemented. The schematic arrangement shown in Figure 6 represents the approach taken in the Aurox Clarity system. Once this optical arrangement has been adopted, it is then necessary to decide how to achieve the required sinusoidal modulation as well as to choose an appropriate light source and suitable camera to record the images. We will now address these three issues.

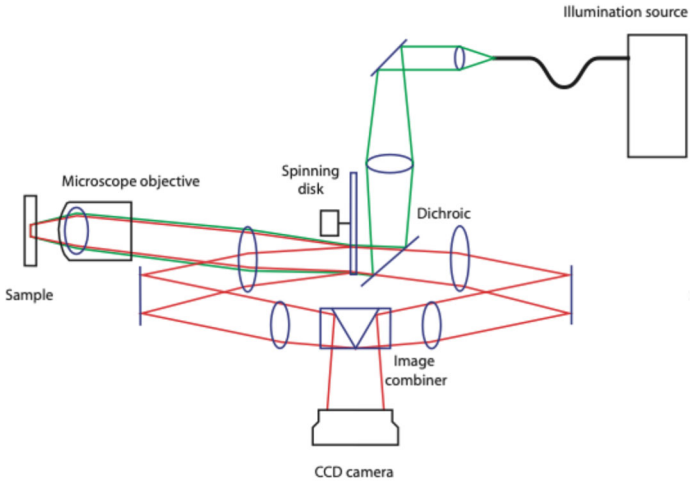

Figure 6. A schematic diagram of the structured illumination and structured detection architecture adopted in the Aurox Clarity system.

The illumination structure.

Although it is the normalized spatial frequency of the sinusoidal illumination pattern – the label -- which determines the optical sectioning strength it is the value of the transfer function, $C(u, \bar{f})$, at this spatial frequency which determines the strength of the labelled optical sectioned image component in the composite image. The design of any imaging system based on this structured illumination and structured detection principle – essentially the choice of grid pitch -- therefore involves a compromise between the desired image contrast and the optical sectioning strength. These considerations have led to the incorporation of three different grid patterns within the Aurox Clarity confocal unit. This system also comprises

four fluorescent imaging channels and Figure 7 shows the axial responses -- variation in signal strength as a function of defocus when imaging a thin fluorescent sheet from an Andor FRAPPA slide – for various objective lenses using the GFP imaging channel (466 nm, excitation; 525 nm emission).

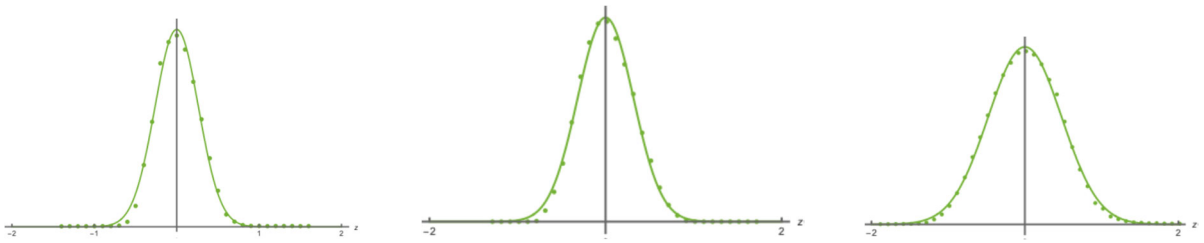

(a) (b) (c)

Figure 7. The axial responses are shown for 100 µm pitch grid for three objective lenses. The result shown in Figure 7(a) was obtained with a Nikon PlanApo l D, 100x, 1.45 NA oil immersion objective, A Nikon Nikon PlanApo l D 60x 1.42 NA oil immersion objective was used for Figure 7(b) whereas the measurement shown in Figure 7(c) were obtained with a Nikon PlanApo l D 40x 0.95 NA dry objective. The full width half maximum (FWHM) of these measurements are 0.62 µm, 0.75 µm, and 1.1 µm respectively.

Figure 8 (a) illustrates the effect of grid pitch by showing the axial response for the Nikon 100x, 1.45 NA oil immersion objective when 100 µm and 200 µm pitch illumination is used. In both cases the GFP channel was used and we see that the half width falls from 0.62 µm 2.84 µm with the larger spaced grade.

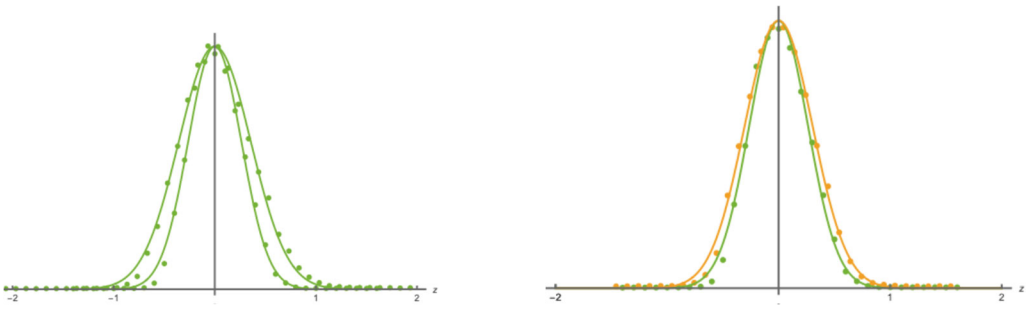

Figure 8. The inner curve of Figure 8((a) shows the axial response with a 100 µm pitch grid. The outer curve shows the same result when a 200 µm pitch grid was used. Figure 8(b) shows the effect of wavelength. In this figure a 100 µm pitch grid was used. The inner curve shows the axial response with the GFP channel whereas the outer curve shows the result when the signal is displayed from the DSRed channel. The full with half maximum (FWHM) increases from 0.62 µm in the GFP case 0.72 µm in the DSRed channel.

The performance of any imaging system depends on wavelength and we emphasise this in figure 8 (b) where the axial responses using the same FRAPPA specimen and 1.45 NA oil objective are presented when imaging using the GFP channel and the DsRed channel (554 nm, excitation; 609 nm emission) on an Aurox Clarity system with a 100 µm grid pitch. As expected, the sectioning strength is weaker at the longer, DsRed, wavelength.

Although it is possible in principle to manufacture a mask with signal transmission it is considerably easier to use one consisting of equally space metallised lines. In this sense the mask is a one-dimensional grid pattern with transmission alternating between zero and unity. In this case, if the pitch of the equal mark-to-space ratio grid is Λ, we may rewrite equation (2) as

$$I(x_0) = \frac{1}{2} - \frac{2}{\pi}\sum_{k=1}^{\infty}\frac{(-1)^k}{2k-1}\cos(2k-1)\frac{2\pi x_0}{\Lambda} \tag{12}$$

and hence

$$I_{\text{section}}(u) = \sum_{k=1}^{\infty}\frac{1}{(2k-1)^2}\, C_1\big(u,(2k-1)\bar{f}\big)C_2\big(u,(2k-1)\bar{f}\big) \tag{12}$$

or, writing out the first few terms

$$I_{\text{section}}(u) = C_1\big(u,\bar{f}\big)C_2\big(u,\bar{f}\big) + \frac{1}{9}\, C_1\big(u,\overline{3f}\big)C_2\big(u,3\bar{f}\big) + \frac{1}{25}\, C_1\big(u,5\bar{f}\big)C_2\big(u,5\bar{f}\big) + \cdots \tag{12}$$

We note that if the grid frequency is chosen so that $3\bar{f} \geq 2$ (or $\Lambda \leq \frac{3}{2}\lambda\frac{\text{M}}{\text{NA}}$) such that only the first term of this expression is non-zero then we have achieved the goal of sinusoidal illumination.

Camera

We will consider two sCMOS cameras pco.edge 10 bi CLHS and pco.edge 9.4 bi CLHS since they represent two different flavors of very similar sCMOS image sensors. They share the same pixel size of 4.6 µm x 4.6 µm, similar resolutions (10 Mpixel and 9.4 Mpixel) with similar 16:9 and 16:10 aspect ratios as sensor format. The quantum efficiency is the same, both sensors are backside illuminated with the addition of deep trench isolations and micro lenses to improve the modulation transfer function. While they look very similar, the pco.edge 10 bi is optimized for larger fullwell capacity to achieve a higher dynamic range and the pco.edge 9.4 bi is optimized for the lowest readout noise, enabling a detection sensitivity which is photon counting like. This can be seen in the low signal histograms in figure 9 where a comparison of the simulation results of two different readout noise sCMOS image sensors which are illuminated with an average signal of four photo electrons. This illustrates the photon counting sensitivity of the lower readout noise image sensor, where the values can be more trusted.

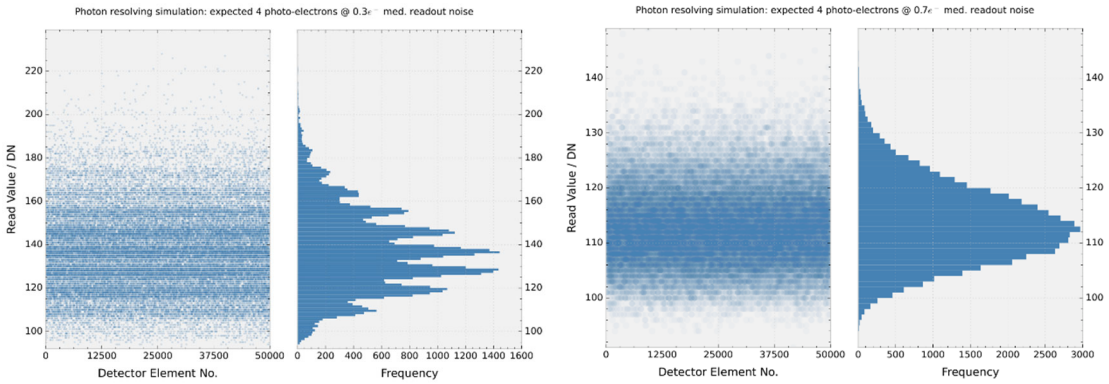

Figure 9. Comparison of simulation results if an average light signal of 4 photo electrons has illuminated the image sensor with left a readout noise of 0.3 [e-] (pco.edge 9.4 bi CLHS) or with right a readout noise of 0-7 [e-] (pco.edge 10 bi CLHS).

Beside the signal-to-noise-ratio performance, there are three more parameters which are very important for the Clarity microscope system. The resolution of 9.4 or 10 Megapixel, the pixel size of 4.6 µm x 4.6 µm and the aspect ratio of appr. 16 : 9 of the image sensor format.

Pixel Size & Resolution

In figure 10 left image, a comparison of two high resolution image sensors is shown at the camera output of a modern microscope with relation to a large image circle (25 mm, dashed green circle fig 10. left image) which is achieved there. Image sensor 1 corresponds to an sCMOS image sensor with 3200 x 3200 pixel and 6.5 µm x 6.5 µm pixel size (large light blue square, fig. 2 left image) and sensor 2 features 4416 x 2368 pixel and 4.6 µm x 4.6 µm pixel size (dark blue rectangle, fig. 2 left image). Clearly the comparison shows that image sensor 1 better covers the given image area at the microscope output. But there is another point of view to this situation. Since both image sensor have different pixel sizes, we have different optical situations regarding achievable resolutions in the sample plane with combination to microscope objective magnifications.

Table 1: Comparison of two selected sCMOS image sensors and their performance data at different microscope magnifications. The data have been generated by using the App Resolution by A. Barlow[2]

parameter	Sensor 1	Sensor 2
resolution	3200 x 3200	4416 x 2368
pixel size	6.5 µm x 6.5 µm	4.6 µm x 4.6 µm
fluroescence wavelength	630 nm	630 nm
microscope magnification	60x	40x
NA	1.2	1.2
Type	immersion oil	immersion oil
optical resolution	0.32 µm	0.32 µm
image pixel pitch	0.108 µm	0.115 µm
Nyquist pixel pitch	0.139 µm	0.139 µm
Sampling	Oversampled + 30.9 nm	Oversampled + 24.2 nm

Table 1 shows a comparison for the two suggested image sensors, and it shows that image sensor 2 with the smaller pixel size allows to use a lower microscope objective magnification with no loss in achievable resolution in the sample plane. For the comparison two immersion oil objectives have been assumed and a fluorescence emission at 630 nm, and both situations, image sensor 1 with larger pixel size and higher magnification (60x), and image sensor 2 with smaller pixel size and lower magnification (40x) result in similar optical resolutions and Nyquist pixel pitches.

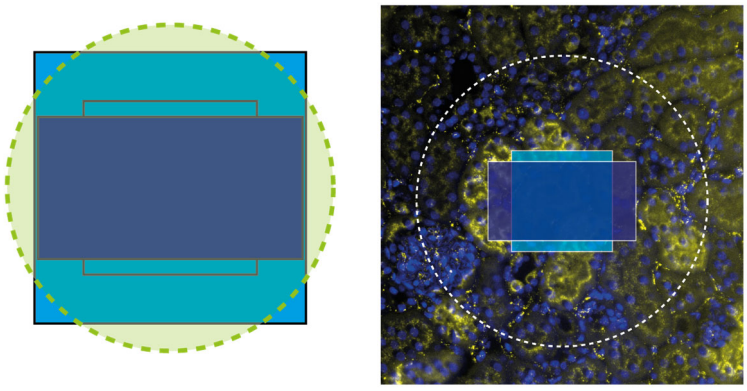

Figure 10. Figure 10 left image: Comparison of the covered areas of two different sCMOS image sensor which have been assumed: Image sensor 1 with 3200 x 3200 pixel resolution and 6.5 µm x 6.5 µm pixel size (large light blue square) and image sensor 2 with 4416 x 2368 pixel resolution and 4.6 µm x 4.6 µm pixel size (dark blue rectangle) in an image circle of 25 mm (dashed light green circle); Figure 10 right image: Comparison of the covered areas of two different sCMOS image sensors 1 and 2 with corresponding different microscope objective magnifications (see above) (image sensor 1 with 60x and image sensor 2 with 40x) in a sample plane with a circular area of 1 mm in diameter (white dashed circle).

If we now look to the conditions in the sample plane, then the comparison of the covered areas for the two image sensor 1 and 2 deliver a different result. As can be seen in Figure 10 right image, if the two image sensors with their microscope objective magnifications are applied to a samples plane, the covered area of image sensor 2 is larger than image sensor 1.This means for example for sample scanning less images are needed and this scales with the scanning of larger areas and additional z-stack recording (see Figure 11). Figure 11illustrates the difference.

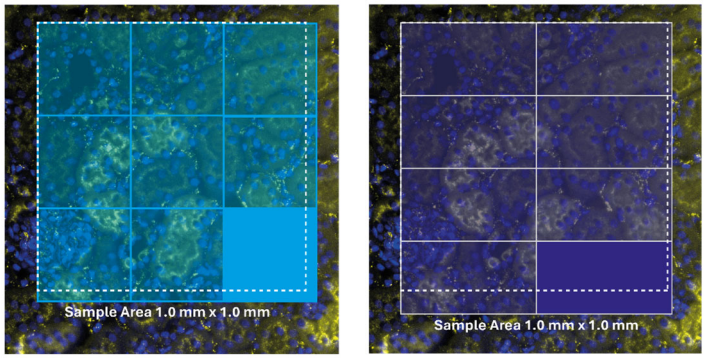

Figure 11. The comparison of image sensor 1 and 2 with their corresponding microscope objective magnifications is assumed. If a sample area of 1 mm x 1 mm should be scanned, image sensor 1 with 3200 x 3200 pixel resolution and 6.5 µm x 6.5 µm pixel size (large light blue square) will have to record in total 9 images to cover the area while image sensor 2 with 4416 x 2368 pixel resolution and 4.6 µm x 4.6 µm pixel size (dark blue rectangle) has to record 8 images only.

If a sample area of 1 mm x 1 should be imaged then image sensor 2 has to detect 8 images compared to 9 images of image sensor 1. Therefore the former advantage of image sensor 1 at the camera port of the microscope is gone.

Image Sensor Format

The image sensor format or aspect ratio of both cameras which seemed to have a disadvantage at the camera port of a microscope turns into an advantage for the special optical sectioning method of laser free confocal microscope system, Clarity. Because the optical sectioning method of the Clarity system is based on aperture correlation, which requires to detect to differently structured illuminated images to be detected at the same time. This means that compared to other SIM methods for optical sectioning it is enough to record one image with two images side by side instead of a lot of images in a time series manner. For that, the maximum achievable resolution of result images is always given by half of the horizontal resolution of the corresponding image sensor as can be seen in Figure 12.

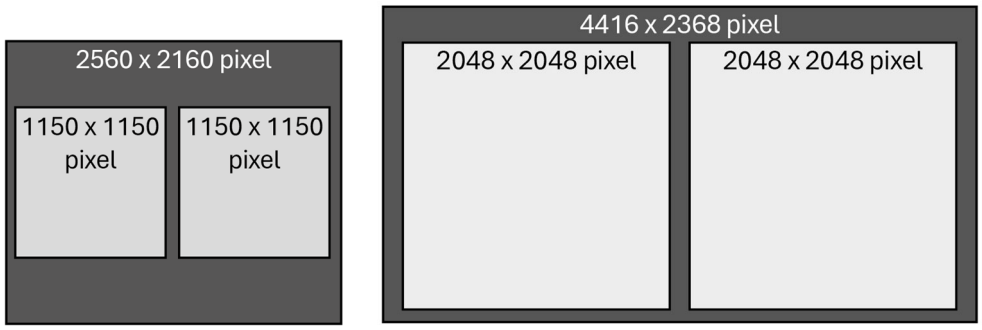

Figure 12. Comparison of useful resolutions if squared microscope images have to be recorded side by side on real existing sCMOS image sensors (drawings are not scaled to real dimensions), left: maximum resolution of 2560 x 2160 pixel (6.5 µm x 6.5 µm pixel size) and right: maximum resolution of 4416 x 2368 pixel (4.6 µm x 4.6 µm pixel size). The final resulting image resolutions are not maximum but nearly maximum (for practical adjustment reason slightly smaller resolutions have been assumed), left: resulting resolution is 1150 x 1150 pixel and right: resulting resolution is 2048 x 2048 pixel.

In Figure 12 two different sCMOS image sensors are compared, which both have been used with the Clarity microscope system, on the left a sensor with an aspect ratio of 5 : 4 and 2560 x 2160 pixel and on the right the before mentioned image sensor 2 which has an appr. aspect ratio of 16 : 9 and 4416 x 2368 pixel. For practical reasons the achievable result image resolutions have not been taken to the extreme half horizontal resolution but near to such that there is some space for image alignment, and it can be seen that a resolution increase from 1150 x 1150 pixel to 2048 x 2048 pixel can be achieved for an extremely fast optical sectioning with 122 frames/s, which represents a significant improvement for the laser free confocal microscope system Clarity.

This can be seen by the high quality result images shown in Figure 13. These two color stain images with the high resolution of 2048 x 1780 pixel. The left hand images show the result images at 40x microscope objective magnification while the right images were obtained at 60x magnification. Both images are shown in false colors without the improvement by deconvolution techniques.

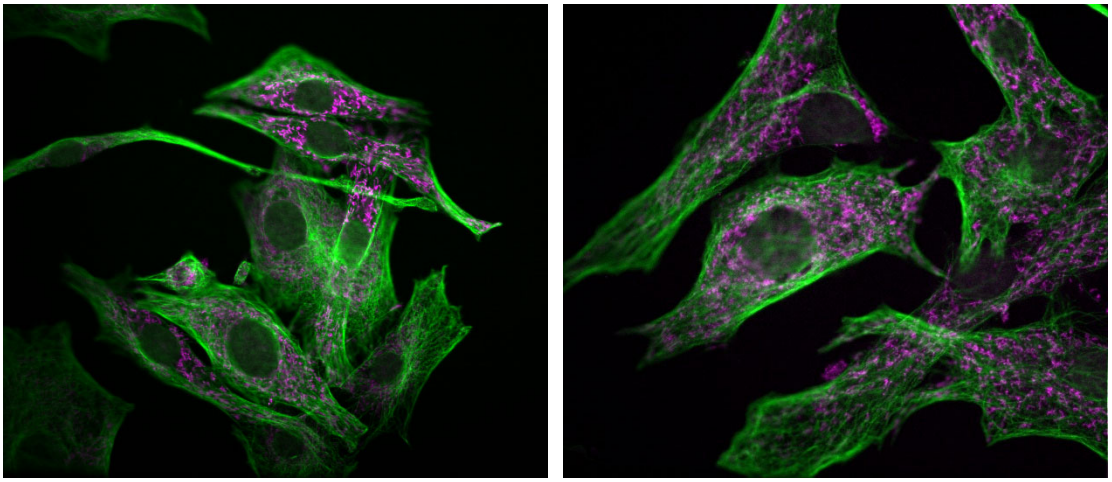

Figure 13. Two stain images with a pco.edge 10 bi CLHS camera attached to a Clarity laser free confocal system at different microscope objective magnifications. Left: 2048 x 1780 pixel single plane image at 40x (no-deconvolution) and right: 2048 x 1780 pixel single plane image at 60x (no-deconvolution, all images have been processed with Huygens Software[3]).

Light source

The Clarity system can be used with any of the X-Cite® light sources (Figure 14). The X-Cite XYLIS II™ is liquid light guide coupled with a broadband spectrum. The X-Cite mini+® is direct coupled with lower power than the XYLIS II, and also a broadband light source. X-Cite TETREM™ is a liquid light guide coupled, 4-channel switchable light source. The term broadband refers to a light source with a broad spectrum where the user cannot turn on and off specific LEDs, and where filters are required to narrow the spectrum to the wavelength of interest. This works for most applications involving fixed cells. Switching speed becomes important in high-throughput imaging and live-cell imaging, where wavelengths need to be switched quickly to preserve sample integrity. For these applications, having a fast-switching light source and using multi-band dichroic and emitter in the filter cube become crucial. When choosing a light source, one should also take into consideration the time it takes for the light to turn on (and to what percent of intensity) after the signal is sent to the LED via TTL or USB. USB signals will always have a delay when compared to TTL. Some factors to consider when choosing the right light source, other than wavelengths required according to fluorophores being imaged, are discussed below.

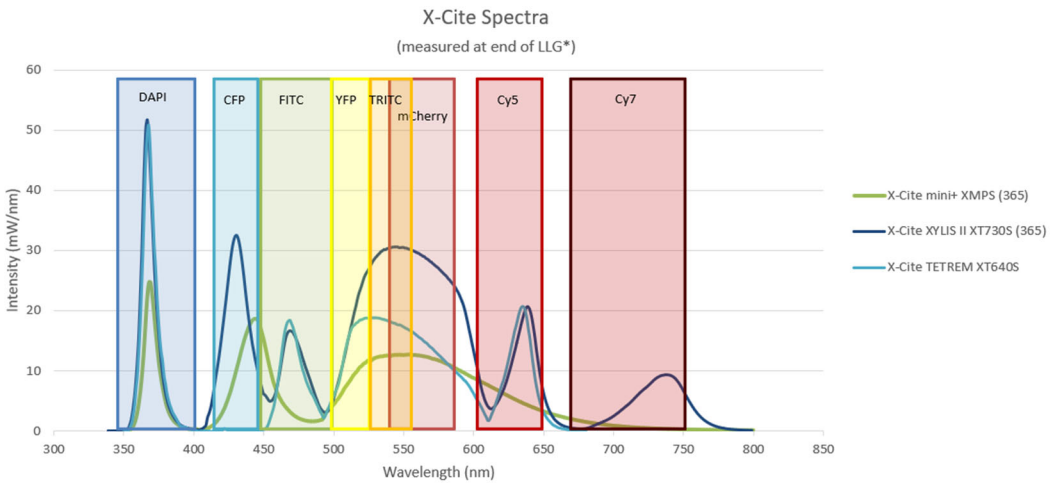

Figure 14. Spectrum of some of the X-Cite light sources that can be used with Clarity system with overlaid with popular fluorophore excitation bands. *For LLG coupled systems, measurements were obtained with a 3mm x 1.5m Liquid Light Guide. For direct coupled systems, measurements were scaled down for realistic comparisons to LLG coupled systems.

Light guide vs. Direct coupled

Light guide coupled light sources provide good uniformity across the field of view (Figure 15), but distance between the light source and the microscope causes losses along the way through the light guide. Using a light guide introduces a Gaussian profile to the beam due to aberration from coupling lenses and the light guide acceptance numerical aperture. This is best mitigated by using the right coupling adaptor. Direct coupled light sources allow all the light from the LED source to go directly into the microscope, but they can be associated with heating and vibrational issues depending on the cooling method used inside the unit, which can have a detrimental effect on live samples and cause image artifacts.

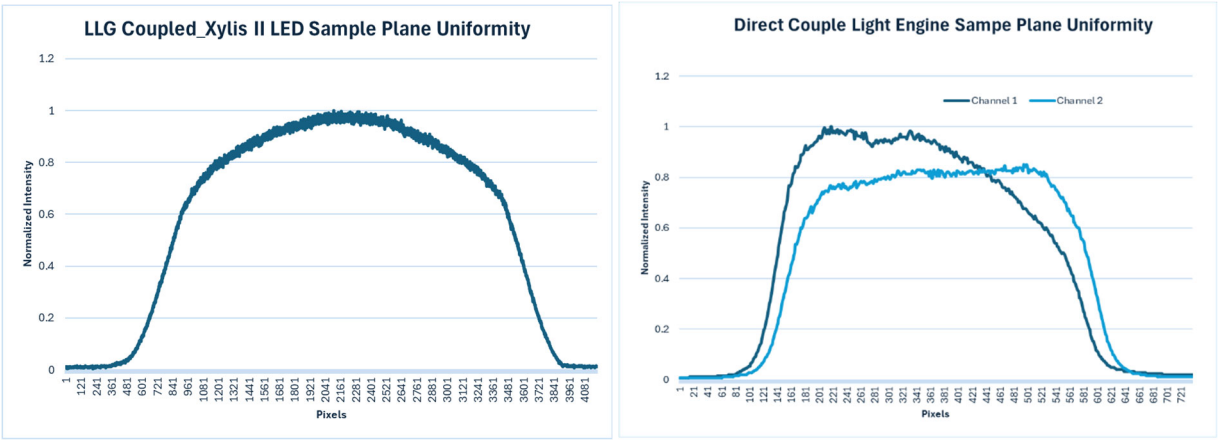

Figure 15. Uniformity of a light source at the sample plane. Fiber coupled uniformity (left) compared to 2 wavelengths of a direct coupled system (right).

Stability/repeatability and thermal management

When illuminating a sample, it is important to ensure every time an LED turns on, the same light dose is reaching the sample (16 top). This allows for reliable data over time during live cell imaging, and also in-between samples of the same experiment.

Contrary to popular belief, LEDs, like lamps heat up. In fact, LEDs are more sensitive to heat when compared to a lamp, which can translate to instability in output and also wavelength drift. Careful thermal management is key to designing a stable LED light source over time, but also at low intensity settings (Figure 16b, bottom).

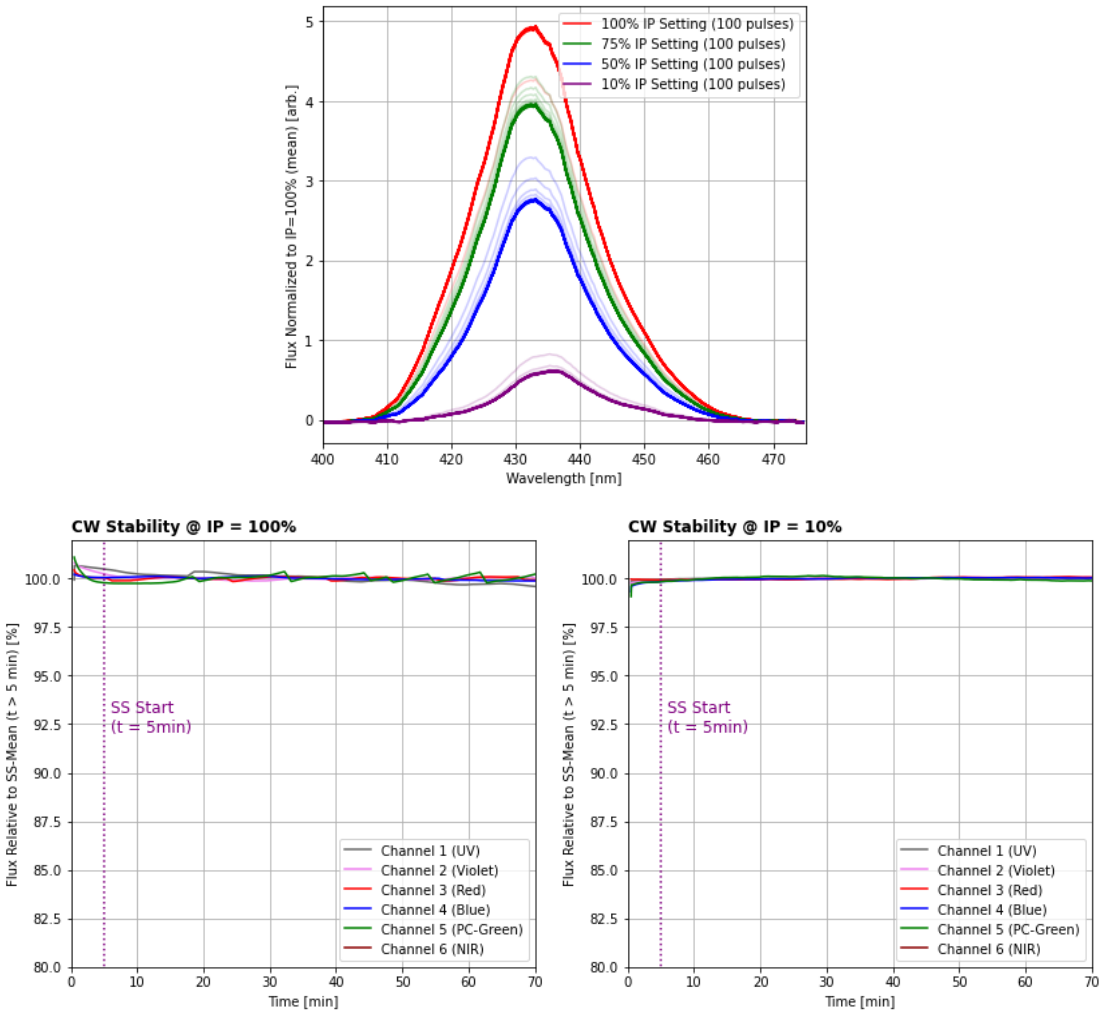

Figure 16. Optical output stability and repeatability. 16a depicts consistent pulse-to-pulse light dose (spectrum and power) delivery over a pulse-train at varying intensities, 40ms on, 60ms off. 16b Steady-state optical output stability of X-Cite LEDs at 100% intensity (left) and 10% intensity settings (right). Measurements were done with LED in continuous mode (CW) seeping across 6 channels. PC-Green indicates a phosphor converted green LED.

Overheating can also lead to wavelength drift over time, which translates to change in efficiency of fluorophore excitation that can skew quantitation of data. Once again, effective thermal management, and/or having a closed-loop-feedback system can assist in keeping the wavelength and power output stable, even with an increase in LED temperature (Figure 17a). If imaging in pulsed mode, effective thermal management can also ensure that despite the duration of pulses, the wavelength will not change, leading to reliable data (Figure 17b).

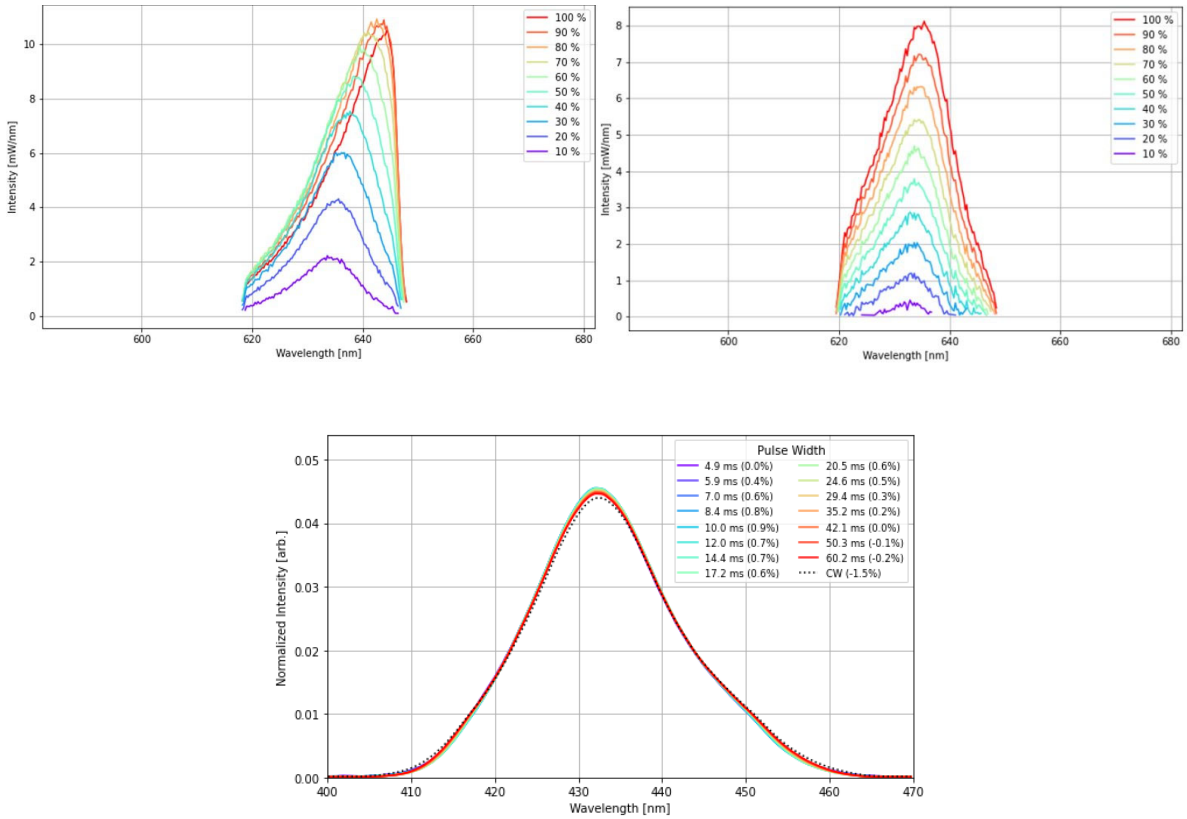

Figure 17. Wavelength stability of LEDs. 17 depicts a light source with wavelength drift over time with increasing LED intensity, leading to increased temperature at the LED (left), and a X-Cite LED with minimal drift in peak wavelength (right). Bottom: Wavelength stability when imaging at several pulse-widths.

Conclusion

We have described a light efficient alternative optical system to provide optical sectioning in optical microscopy. This approach, unlike that of the traditional confocal point-source point-detector geometry, does not require laser illumination or scanning. Since it is light efficient it is able to take advantage of the availability of the latest generation of LED based sources and development in sCMOS camera technology.

ACKNOWLEDGEMENTS

TW would like to acknowledge the assistance of Rimas Juškaitis and Jonathan Parker in obtaining the data presented in this paper. KA would like to acknowledge Kevin Joseph, Joe Lee and Pit Chiu for the images and data presented in this paper.

REFERENCES

[1] Wilson, T.; Juškaitis, R.; Neil, M.A.A. and Kozubek, M.; “Confocal microscopy by aperture correlation”, Optics Letters, Vol. 21, Issue 23, pp. 1879-1881 (1996); https://doi.org/10.1364/OL.21.001879
[2] Software Application “Resolution” by Andrew Barlow: https://play.google.com/store/apps/details?id=com.Barlowax.resolutionfragments
[3] Huygens Software, by Scientific Volume Imaging, https://svi.nl/Huygens-Software